Saafi, Mohamed and Tang, Pik Leung and Fung, Jason and Rahman, Mahbubur and Liggat, John (2015) Enhanced properties of graphene/fly ash geopolymeric composite cement. Cement and Concrete Research, 67. 292–299. ISSN 0008-8846 , http://dx.doi.org/10.1016/j.cemconres.2014.08.011

Enhanced properties of graphene/fly ash geopolymeric composite cement

Mohamed Saafi[1]* Leung Tang[2], Jason Wang[1], Mahbubur Rahman[1] and John Liggat[3]
[1]Department of Civil and Environmental Engineering, University of Strathclyde, G4 0NG, UK
[2]Agilent Technologies, -EH12 9DJ, UK
[3]Department of Pure and Applied Chemistry, University of Strathclyde, G4 0NG, UK

Abstract

This paper reports for the first time the incorporation of in-situ reduced graphene oxide (rGO) into geopolymers. The resulting rGO-geopolymeric composites are easy to manufacture and exhibit excellent mechanical properties. Geopolymers with graphene oxide (GO) concents of 0.00, 0.10, 0.35 and 0.50% by weight were fabricated. The functional groups, morphology, void filling mechanisms and mechanical properties of the composites were determined. The Fourier transform infrared (FTIR) spectra revealed that the alkaline solution reduced the hydroxyl/carbonyl groups of GO by deoxygenation and/or dehydration. Concomitantly, the spectral absorbance related to silica type cross-linking increased in the spectra. The scanning electron microscope (SEM) micrographs indicated that rGO altered the morphology of geopolymers from a porous nature to a substantially pore filled morphology with increased mechanical properties. The flexural tests showed that 0.35-wt% rGO produced the highest flexural strength, Young's modulus and flexural toughness and they were increased by 134%, 376% and 56%, respectively.

Keywords: C. Mechanical Properties, D. Alkali Activated Cement, E. Composite, D, Reinforcement.

* Corresponding author: m.bensalem.saafi@strath.ac.uk, Tel: 44 (0) 141 548 4569

1. Introduction

In recent years, considerable research has been aimed at the development of fly ash based geopolymers. This is driven by the need to reduce or complement the ordinary Portland

cement (OPC) consumption in the construction industry. OPC is major contributor to green-house gases when compared to geopolymers. Geopolymers in general emit less green-house gases due to their lower calcium carbonate-based raw materials and production temperature. Geopolymers are inorganic polymers synthesized via a chemical reaction between a highly alkaline solution and the Si-Al minerals present in the fly ash. This results in a 3-D polymeric network consisting of Si-O-Al-O bonds with the formula of $M_n\left[-\left(SiO_2\right)_z - AlO_2\right]wH_2O$ where M is an alkaline element, n is the degree of polymerization, z is a value between 1 and 32, and w is the hydration extent, which is a function of the type and amount of the alkaline solution used [1]. The most commonly used alkaline solution is a mixture of sodium silicate (Na_2SiO_3) and sodium hydroxide (NaOH) with a Na_2SiO_3/NaOH ratio between 1.5 and 3 [2]. The processed type F fly ash based geopolymers exhibit mechanical properties similar to those of OPC but with better performance under severe environmental conditions. For example, it has been reported that geopolymers exhibit excellent resistance to acid and sulfate attack when compared to OPC due to the lower calcium content of the fly ash [3-5]. Fly ash based geopolymers are also fire resistant binders. According to Pan el al. [6], geopolymers are inherently fire resistant due their polymeric-silicon-oxygen-aluminum framework. Pan et al. [6] and Duxson et al. [7] have shown that geopolymers can sustain high temperatures (up to 800^{o}C) with little gel structural degradation.

OPC and geopolymers are typically brittle and characterized by low tensile strength and fracture toughness. To combat this, OPC and geopolymers are often reinforced with micro and nano fibers. For example, fibers such as steel, polypropylene (PP), polyvinyl chloride (PVC) and basalt fibers have been found to be particularly effective in controlling crack propagation and enhancing the flexural strength and the fracture energy of geopolymers [8]. These enhanced properties were mainly attributed to the fiber bridging effect during both micro and macro cracking of the geopolymeric matrix [8]. The mechanical interlocking at the

55 fiber-matrix interface and chemical bonding between the fiber and the matrix both play a role
56 in strengthening and toughening of the geopolymeric matrix [9].

57 Recently, carbon nanotubes (CNTs) were adopted as a reinforcement for geopolymers.
58 The unique properties such as high elastic modulus and tensile strength and high aspect ratio
59 make CNTs an ideal candidate for reinforcement. Mackenzie and Bolton [10] investigated
60 the tensile strength of potassium-based aluminosilicate (clay) geopolymers containing single
61 walled carbon nanotubes (SWCNTs) at concentrations of 0.20, 0.25 and 0.35-wt%. The
62 tensile strength results were inconsistent. The tensile strength decreased, and then increased
63 before it began to decrease again. Saafi et al. [11] studied the multifunctional properties of
64 geopolymers containing multiwalled carbon nanotubes (MWCNTs). Their experimental
65 results indicated that the incorporation of MWCNTs up to 0.5-wt% enhanced the flexural
66 strength, the Young's modulus, the flexural toughness and the fracture energy of
67 geopolymers. This improvement was due to a variety of CNT strengthening and toughening
68 mechanisms, including high resistance to crack coalescence, crack deflection at the
69 CNT/matrix interface, inducing and bridging of multiple cracks and CNT pullout on the
70 fractured surfaces [12].

71 A non-aggregated dispersion of CNTs in aqueous liquid media is a prerequisite for their
72 use as reinforcing fillers in cement and geopolymer based composites. However, dispersion
73 of CNTs in water is highly challenging as van der Waals forces between the CNTs create
74 bundles and agglomerates. For CNTs, this phenomenon reduces the workability and
75 mechanical properties of composites [13, 14]. Graphene offers many benefits over CNTs,
76 including higher surface area (due to its 2-dimensional structure) and strong mechanical
77 interaction with the hosting matrix resulting from the wrinkling [15]. However, graphene
78 sheets exhibit very low dispersibility in polar liquids due to their high surface area and surface

79 energy and, as a result, they agglomerate and stick to each other, thereby reducing their
80 reinforcement effects when agglomerated [16].

81 Graphene oxide (GO), the oxidized form of graphite has been considered as a precursor for
82 bulk-scale production of low-cost graphene-based materials [17]. GO sheets contain a large
83 concentration of hydroxyl, epoxide, carboxyl and carbonyl functional groups [18]. These
84 functional groups are compatible with water and therefore the GO is highly dispersible in
85 polar liquids [19]. GO-based fillers were incorporated into various plastic and organic
86 composites [20, 21]. The improved mechanical properties of these composites were attributed
87 to the high specific surface area and excellent mechanical properties of GO sheets [21].

88 In view of these outstanding properties, the integration of graphene into geopolymers can
89 significantly improve their properties and provide them with self-sensing capabilities. The
90 objective of this paper is to investigate the mechanical properties, chemical functional group
91 changes and morphological changes of geopolymers containing reduced GO (rGO) sheets at a
92 variety of loadings. The properties discussed herein are the morphology characteristics, the
93 flexural strength, the Young's modulus, the flexural toughness and the void and pore filling
94 mechanisms together with chemical changes associated with the alkaline reduction of GO.

95 **2. Experimental program**

96 *2.1. Materials*

97 Class F fly ash was used to process the rGO-geopolymeric composites. The chemical
98 composition of the fly ash is given in Table 1. Based on the size distribution tests conducted
99 by the supplier, 70% by weight of the total type F fly ash spherical particles were between 0.2
100 and 5μm in diameter.

101 Hydrophilic and oxygenated 1.1 nm thick pristine GO sheets (0.5 – 5μm with purity higher
102 than 90%, supplied by Supermarket®) were employed in this study. The required GO content
103 was dispersed in deionized water by using a 100W Cell Disruptor for 1.5 hours. The plain

104 geopolymeric matrix had a bulk of density of 2.0 g/cm^3 and composed of 72-wt% fly ash, 20-
105 wt% of sodium silicate (Na_2SiO_3 with 29.4% SiO_2, 14.7% NaO_2 and 59.9% H_2O) and 8-wt%
106 of 10M sodium hydroxide (NaOH). The (Na_2SiO_3 + NaOH) to fly ash ratio was 0.39.

107 *2.2. Fabrication of rGO-geopolymeric composites*

108 To chemically reduce the GO sheets during mixing and curing, the dispersed pristine GO
109 sheets were first added to 100g of NaOH solution (10M) and mildly sonicated for 1 hour.
110 The stable and heterogeneous mixture was then mixed with the fly ash and the left over
111 chemicals (Na_2SiO_3 + NaOH) for 1 minute. Subsequently, the mix was subjected to
112 sonication for 3 minutes prior to casting the beams. Geopolymeric beams (50 mm x 50 mm x
113 350 mm) containing different concentrations of rGO (0.00, 0.10, 0.35 and 0.50-wt%) were
114 prepared. The molded geopolymeric beams were first cured at a room temperature of 25^{o}C for
115 2 hours and then placed in an oven for 24 hours at constant temperature of 60^{o}C.

116 *2.3. Morphology and chemical characterization*

117 The morphology of the rGO-geopolymeric composites and the rGO sheets were examined
118 with a scanning electron microscope (SEM). SEM observations were also performed on the
119 rGO-geopolymeric suspensions in order to identify their morphology during processing. An
120 Agilent Technologies Exoscan 4100 Fourier transform mid-infrared spectrometer, with
121 diffuse sample interface, was used to collect infrared diffuse spectra. The instrumental
122 conditions for spectral collection were 128 scans at a resolution of 8 cm^{-1}. The spectral
123 changes both in terms of size and position were used to identify the processes and chemical
124 changes in the pristine GO sheets and geopolymeric composites. In addition, the
125 geopolymeric gels and the rGO sheets were also studied with particular attention paid to the
126 chemical bonding and functional groups present.

127

128

129 *2.4. Mechanical characterization*

130 In total, 10 geopolymeric beams per rGO content were prepared for the mechanical
131 characterization. The beams had a clear span of 210 mm and a distance between the two
132 loading contacts of 70 mm. The beams were subjected to four-point bending tests to
133 determine the mechanical properties; namely, flexural strength, Young's modulus and flexural
134 toughness. The four-point bending tests were conducted under displacement control with a
135 rate of 0.05 mm/min. During testing, load and deflection at the center were recorded
136 continuously. The flexural strength (σ_f) and the Young's modulus (E) were calculated as:

137 $$\sigma_f = \frac{3Pa}{b^3} \quad (1)$$

138 $$E = m\frac{a\left(3l^2 - 4a^2\right)}{4b^4} \quad (2)$$

139 where P is the maximum applied load, l is the length of the beam between the supports, a is
140 the distance between the support and the loading point, b is the width and thickness of the
141 beam and m is the slope of the tangent to the straight-line portion of the load-deflection curve.
142 The flexural toughness of the beams is the total area under the stress-strain curve obtained
143 from Eqs. 1 and 3, where Eq. 3 is given by:

144 $$\varepsilon = \frac{12b\Delta}{3b^2 - 4a^2} \quad (3)$$

145 where ε is the tensile strain and Δ is the displacement recorded by the LVDT.

146 **3. Results and discussion**

147 *3.1. FTIR analysis and chemical characterization*

148 Figure 1 depicts the FTIR spectrum of the fly ash, (black dashed line), pristine GO sheets
149 (yellow solid line), plain geopolymers (red dash-dotted line) and rGO-geopolymers with 0.35-
150 wt% (blue dotted line). The FTIR spectrum of the fly ash is dominated by two overlapping
151 peaks corresponding to Si-O (doublet) and Al-O functional groups or bonds in the range of

800 to 1200 cm^{-1}. These groups are clearly observed in the spectra as shown in Fig. 2. The Si-O and Al-O overlapping (negative) restrahlen peaks represent the main mineral content of the fly ash (see Table 1) and are much greater than the C-H stretching modes that are the two downward peaks in the spectral region of 3000-2850 cm^{-1}. The organic content (C-H) of the fly ash is much smaller than the mineral content (Si-O and Al-O) in good agreement with Table 1. The restrahlen peak absorbances at ~1800-1700 cm^{-1} are the result of the presence of other organic functional groups in the fly ash, namely carbonyl type species. Finally, a variety of hydrogen bonded -OH functional groups derived from Al-OH, Si-OH and C-OH exist in the dried fly ash as evidenced by the complexity of the peak shape in –OH functional group (3000-3700 cm^{-1}).

From Fig. 1, it can be seen that the pristine GO sheets contain high concentrations of hydroxyl (at 3000-3700 cm^{-1} and ~1600 cm^{-1}) and carbonyl (~1700 cm^{-1}) functional groups. The FTIR spectrum of the unreduced GO sheets also displays the existence of methyl/methylene (CH_2/CH_3) stretches between 3000 and 2800 cm^{1}. These groups are concentrated at the edges of the GO sheets.

For both geopolymers (red line or blue line in Fig. 1 – with or without GO), the alkaline activator (NaOH + Na_2SiO_3) changed the fly ash hydroxyl spectral absorbance peak shape from a complex distribution to a near homogeneous hydroxyl functional group. These chemical changes are due to the loss of the peak as a consequence of bond destruction. Figure 1 indicates a distinct shape change for the –OH from the base fly ash to the geopolymer. It also shows that the alkaline activator changed the distribution of the Al-O/Si-O regions at 800-1200 cm^{-1} for both geopolymers. The addition of sodium silicate increased the relative concentration of Si-O in the geopolymeric matrix. As expected due to the presence of rGO, the rGO geopolymers exhibited higher organic contents at ~1500 cm^{-1} as compared to the plain geopolymers. These negative/derivative peak shapes are caused by concomitant

changes in the refractive index with the absorbance changes as shown by the downward negative peaks in the indicated region in figure 1. This is very common in materials that contain high silicate content or similar and/or contain highly scatteruing components such as flyash or graphene oxide.. . From the FTIR spectrum of the rGO-geopolymetric matrix, it can be seen that the GO has undergone chemical reduction of the hydroxyl and carbonyl functional groups, whereas the unreactive C-H peaks at 1500 cm^{-1} remained largely unchanged due to their inert nature.

Figure 2 shows the FTIR spectra between 2000-650 cm^{-1} of both the plain and the rGO reinforced geopolymers. As shown in this figure, the presence of the rGO in the geopolymeric matrix increased the moderately absorbing band at ~1425 cm^{-1}, this can be assigned to a C-H vibration. In addition, the Si-O bonds increased the absorbance at 1000-1200 cm^{-1} as a direct result of the chemical reaction of the sodium silicate with the matrix components creating new Si-O_2 based cross-linking with fly ash or rGO. The change in absorbance is marked large considering the rGO addition was a mere 0.35wt%

Figure 3 further confirms that the pristine GO sheets have been reduced during the processing of the geopolymers. This figure compares the FTIR spectra of the isolated unreduced/pristine GO sheets with the difference spectra of the geopolymer with and without the incorporation of 0.35wt% GO. The dotted blue line is the difference between each single point of the spectra presented in Fig. 3 for the full spectral region. As can be seen from this figure, there is a clear attenuation of hydroxyl and carbonyl functionalities between 3000 and 3750 cm^{-1} and, between 1650 and 1800 cm^{-1}, respectively. High attenuation of the hydroxyl and carbonyl groups inidicating reduction of GO by the alkali NaOH [22, 23] as shown in the difference spectra. The non-reducible functional groups of the GO are still present in the difference spectra at 3000-2850 cm^{-1} and at 1200-1500 cm^{-1}, these are the unreactive C-H type bonds. Previous studies have shown that during processing with NaOH or strong alkali,

202 the GO sheets undergo deoxygenation and the number of carbonyl and hydroxyl groups are
203 then reduced. This leads to the formation of highly reducedGO sheets (rGO) with mechanical
204 and electrical properties superior to those of pristine GO sheets [22, 23]. The authors suggest
205 that the GO incorporated into the geopolymer actually contains the in-situ reduced-GO cross-
206 linked graphene based material within the geopolymer matrix thereby increasing mechanical
207 and electrical properties. Additionally greatly lowering porosity.

208 The mechanical properties of the rGO-geopolymeric composites are highly dependent on
209 the physical and chemical interactions between the rGO and the matrix. These interactions
210 include both mechanical and chemical covalent bonding. The mechanical interaction is due to
211 the mechanical interlocking between the textured (wrinkled) morphology of the rGO sheets
212 and the matrix. The Si-O covalent bond absorbance augmentation is likely to be the cross-
213 linking bridging between the fly ash and the rGO sheets. The authors suggest that the *in-situ*
214 cross-linked particles in the form of $[\text{-Si-O-}]_x[\text{rGO}]_y[\text{-O-Si-}]_z$ (with $x \geq 1$, $y \geq$ and $z \geq 0$) is
215 formed in the rGO-geopolymeric matrices. The silicon has the ability to further bond to the
216 fly ash or rGO, this creates a diverse particle size, shape and morphologies enabling virtually
217 any pore or void to be filled. Moreover unreacted hydroxyl groups on the GO or fly ash can
218 undergo further cross-linking to become larger crack filling and bridging particles.

219 *3.2. Morphology*

220 The morphology of the fly ash is well known and is a wide distribution of mostly spherical
221 particles that encompasses the submicron to the micron range. These particles are the
222 dominant base for both types of geopolymers and are highly siliceous. Figure 4a shows the
223 SEM micrograph of the rGO sheets, clearly there is a highly textured morphology enabling
224 the rGO to morph around complex shapes and interact mechanically. The chemical alkaline
225 reduction of GO to rGO (reduced form) removes the oxygen rich functional groups as well as
226 causing the high degree of wrinkling and folding [24]. Wrinkles have a positive effect on the

mechanical properties of rGO reinforced geopolymers, as they tend to improve the interlocking mechanism within the matrix [25]. Figures 4b, 4c and 4d show the morphology of the geopolymeric suspensions containing 0.35-wt% rGO. In Fig. 4b, the sub-micron fly ash spheres are randomly deposited on the rGO sheets. The rGO sheets exhibited random holes and tearing. From Fig. 4b, it can be seen that the size the submicron fly ash spheres matches the size of the holes, suggesting that some of the particles pierced the rGO sheets during processing, resulting in random holes. Fig. 4c shows the fly ash particles covered with thin rGO sheets, forming hybrid clusters. This can be attributed to the effect of cross-linking and functionalization on the surface area of the rGO sheets and the fly ash particles [26, 27]. The exchange between the two materials typically occurs through electric induction (also known as polarization) causing the rGO sheets to adsorb onto the fly ash particles. The strain induced by the largest fly ash particles also caused the folding of the flexible rGO sheets around the largest fly ash particles, producing shapes like a "mushroom" as shown in Figs. 4c and 4d. One possible interpretation for this observation is that the rGO sheets inherently contain both crystalline and amorphous regions. The amorphous region is less stable, more soluble and relatively disordered thus becomes more amenable to deform when the fly ash particles push against it.

Figures 4c and 4d also show that the pores and voids were substantially filled and bridged at 0.35-wt%, partially due to the formation of the cross-linked particles. The pore filling with the malleable rGO sheets also reduced the porosity and presence of voids. Additionally, the small scraps of rGO sheets that were moved by the fly ash particles also filled and bridged the voids and hollow spaces in the matrix as depicted in Fig. 5.

3.3. Mechanical characterization

Figure 6 shows the load-deflection responses of the geopolymeric beams. The beams were initially preloaded up to a deflection of 0.2 mm to ensure good contact with the load and

support points. The load-deflections results indicated the significant increase in stiffness and load-carrying capacity of the beams due to the addition of rGO sheets. This is attributed to the stiffness and surface area of the rGO sheets. The wrinkled texture of the rGO sheets also played a positive role in the load transfer between the rGO sheets and the geopolymeric matrix, as it tends to enhance the mechanical interlocking coupled with chemical cross-linking type bonding.

The deflection at failure decreased as the rGO sheet content increased. This can be explained as follows (see Fig. 7): at low rGO sheet contents, the sheets are generally separated and randomly dispersed within the matrix with a slight negative effect on the mechanical deformation. At medium rGO contents, the sheets are joined together with some overlapping each other, producing stiff plates rigidly bonded to the matrix. In this case, the matrix is restrained from movement and as a result the deflection is reduced. Severe restacking of sheets occurs at high rGO sheet contents due to van-der-Waals forces (van-der-Waals forces from NaOH-induced attenuation of hydroxyl groups) where the sheets are stacked on top of each other to form rigid laminates. This further restricts the movement of the matrix, causing the beams to fail in a brittle manner. This behavior has also been found in other graphene-based polymer composites [28, 29].

The average mechanical properties are given in Fig. 8. A noticeable flexural strength gain of 49%, 130% and 134% was achieved for beams with rGO sheet concentrations of 0.10, 0.35 and 0.50-wt%, respectively. A significant increase in stiffness was also obtained. The increase was about 107%, 365% and 376% for rGO contents of 0.10, 0.35 and 0.50-wt%, respectively. The flexural toughness was improved by 12%, 56% and 48% for rGO contents of 0.10, 0.35 and 50-wt%, respectively. The geopolymers with 0.35 and 0.5-wt% rGO exhibited somewhat similar mechanical properties, indicating a mechanical percolation threshold was achieved at 0.35-wt%. These results are in line with previous studies on

graphene composites [30, 31]. These studies have shown that graphene sheets can enhance the mechanical properties of composites at significantly lower graphene concentrations in comparison to CNTs. For example, 0.125-wt% of graphene increased the tensile strength and the Young's modulus of polymers by 45% and 50%, respectively, whereas, 1-wt% of CNTs increased the tensile strength and the Young's modulus of polymers by 15% and 30%, respectively [30].

3.4. Toughening and load transfer mechanisms

The rGO morphology and the shear lag model can be used to quantify the load transfer mechanism in the rGO-geopolymeric composites. The relationship between the strain ε_p in the rGO sheet and the geopolymeric matrix strain ε_m, can be written as [32]:

$$\varepsilon_p = \varepsilon_m \left[1 - \frac{\cosh\left(ns \frac{x}{l} \right)}{\cosh\left(n\, s/l \right)} \right] \tag{4}$$

$$n = \sqrt{\frac{2G_m}{E_p} \frac{t}{T}}$$

where G_m is the shear modulus of the matrix, E_p is the Young's modulus of the rGO sheet, l is the length of the rGO sheet in the x direction, t is the thickness of the rGO sheet, T is the total thickness of the matrix and s is the aspect ratio of the rGO sheet (l/t) in the x direction. In Eq. (4), the parameter n is an effective measure of the interfacial stress transfer efficiency and the product ns depending on both the morphology of the rGO sheet and the degree of interaction with the hosting geopolymeric matrix [32].

The morphology of the wrinkled rGO sheet shown in Fig. 6a can be characterized by the wavelength λ and the amplitude A of the wrinkles as [33]:

$$\lambda^4 = \frac{4\pi^2 \nu (tl)^2}{3(1-\nu^2)\varepsilon} \tag{5}$$

298 $$A^2 = \left[\frac{16\varepsilon\nu}{3\pi^2\left(1-\nu^2\right)}\right]^{1/2} tl \quad (6)$$

299 where ν is the Poisson's ratio of the rGO sheet and ε is the compressive strain in the rGO
300 sheet from the exfoliation process.

301 The shear stress between the rGO sheet and the geopolymeric matrix is given by [32]:

302 $$\tau = nE_p\varepsilon_m \frac{\sinh\left(ns\frac{x}{l}\right)}{\cosh\left(ns/2\right)} \quad (7)$$

303 As can be seen from Eqs. (4), (5), (6) and (7), the high aspect ratio $s = l/t$, the Young's
304 modulus E_p and the morphology of the rGO sheet are the main key factors that significantly
305 contributed to the improved mechanical properties of rGO reinforced geopolymers
306 composites .

307 The toughening mechanism in graphene composites is not well understood and research on
308 this topic is limited. This can be attributed to the difficulty of identifying crack pinning or
309 crack bridging by the graphene sheets using traditional analysis tools such as SEM [34].
310 Rafiee et al. [31] have shown that the toughening mechanism in composites reinforced with
311 graphene is different from that reinforced with CNTs. In CNTs, the toughness is dominated
312 by the crack-bridging mechanism where the energy is dissipated by the frictional pullout of
313 the bridging CNTs from the matrix. However, in graphene, the toughening mechanism is
314 crack deflection. In this case, microcracks are deflected and twisted when they run into a
315 rigid graphene sheet. Rafiee et al. [31] reported that this mechanism increases the total
316 fracture surface leading to greater energy absorption. Although further validation studies are
317 needed to identify the toughening mechanism, the experimental results presented herein
318 suggest that crack deflection may have occurred in the rGO-geopolymeric composites and it
319 is reflected in their high Young's modulus and flexural toughness (see Fig. 8).

320 **4. Conclusions**

New rGO-geopolymeric composites with enhanced properties were successfully produced using the same mixing method used to make OPC. The interaction of the GO sheets with the alkaline solution used to process the geopolymeric composites yielded highly reduced and cross-linked GO sheets. The addition of these rGO sheets into geopolymers at very low contents simultaneously improved the mechanical properties and reduced the overall porosity of geopolymers. The malleable rGO sheets and the small scraps of rGO sheets that were moved by the fly ash particles filled the voids and hollow spaces in the matrix. The incorporation of rGO sheets improved the mechanical properties of the geopolymeric composites as a result of their 2-dimensional structure and good chemical bonding with the matrix. The rGO concentration of 0.35-wt% yielded the highest mechanical properties. At this concentration, the flexural strength and Young's modulus increased by 134% and 376%, respectively. A moderate increase in toughness (as much as 56%) was obtained due to the restacking of the rGO sheets and the formation of stiff hybrid of rGO-fly ash fillers within the matrix. The rGO-geopolymeric composites can be an environmental friendly and economical alternative to OPC due to their low green-house gas emissions and improved mechanical properties. The *in-situ* reduction of GO makes geopolymers ideal candidates for high performance and (potentially) self-sensing structural materials for various applications such as bridges, roadways and smart structures with inherent increased durability due their near pore-free morphology.

References

[1] Sakulich AR. Reinforced geopolymer composites for enhanced material greenness and durability. Sustainable Cities and Society 2011*;* 1:195-210.

[2] Hardjito D. Studies on fly ash-based geopolymer concrete. PhD thesis 2005, Curtin University of Technology, Australia.

345 [3] Bakharev T. Resistance of geopolymer materials to acid attack. Cement and Concrete
346 Research 2005*;* 35(5): 658-670.
347 [4] Bakharev T. Durability of geopolymer materials in sodium and magnesium sulfate
348 solutions. Cement and Concrete Research 2005*;* 35(6): 1233-1246.
349 [5] Shankar HS and Khadiranaikar RB. Performance of geopolymer concrete under severe
350 environmental conditions. International Journal of Civil and Structural Engineering 2012;
351 3(2): 396-407.
352 [6] Pan Z, Sanjayan JG and Collins F. Effect of transient creep on compressive strength of
353 geopolymer concrete for elevated temperature exposure. Cement and Concrete Research
354 2014*;* 56: 182-189.
355 [7] Duxson P, Lukey GC and van Deventer JSJ, Thermal evolution of metakaolin
356 geopolymers: part 1—physical evolution. Journal of Non-Crystalline Solids 2006; 352(52-
357 [8] Uddin F, Shaik A. Review of mechanical properties of short fibers reinforced geopolymer
358 composites. Construction and Building Materials 2013; 43: 37-49.
359 [9] D.P. Dias DP, Thaumaturgo C. Fracture toughness of geopolymeric concretes reinforced
360 with basalt fibres. Cement and Concrete Composites 2005, 27: 49–54
361 [10] Mackenzie KJD, Bolton MJ. "Electrical and mechanical properties of aluminosilicate
362 inorganic polymer composites with carbon nanotubes. Journal of Material Sciences
363 2009; 44(11): 2851-2857.
364 [11] Saafi M, Andrew K, Tang PK, McGhon D, Taylor S, Rahman M, Yang S, Zhou X.
365 Multifunctional properties of carbon nanotube/fly geopolymeric nanocomposites.
366 Construction and Building Materials 2013; 49: 46-55.
367 [12] Xia Z, Riester L, W.A Curtin WA, Lia H, Sheldon BW, Liang J, Chang B, Xu JM.
368 Direct observation of toughening mechanisms in carbon nanotube ceramic matrix
369 composites. Acta Materialia 2004; 52 (4): 931-944.

370 [13] Collins F, Lambert J, Duan WH. The influence of admixtures on the dispersion,
371 workability, and strength of carbon nanotube-OPC paste mixtures. Cement and Concrete
372 Composites 2012; 34(2): 201–207.
373 [14] Abu-Al-Rub RK, Tyson BM, Yazdanbakhsh A, Grasley, Z. Mechanical properties of
374 nanocomposite cement incorporating surface-treated and untreated carbon nanotubes and
375 carbon nanofibers. ASCE Journal of Nanomechanics and Micromechanics 2012; 2(1): 1-
376 6.
377 [15] Porwal, H., Grasso S, Reece M. Review of graphene–ceramic matrix composites.
378 Advances in Applied Ceramics 2013; doi 10.1179/1743676113Y.0000000095.
379 [16] Yang Y, William R, Xinyu, Huang X, Li X. Enhancing graphene reinforcing potential in
380 composites by hydrogen passivation induced dispersion. Scientific Reports 2013; 3:
381 2086; doi: 10.1038/srep02086.
382 [17] Zhu Y, Murali S, Cai W, Li X, Won SJ, Potts, JR, Ruoff RS. Graphene and graphene
383 Oxide: synthesis, properties and applications. Advanced Materials 2010; 22(35), 3906–
384 3924.
385 [18] Stankovich S, Piner RD, Nguyen ST, Ruoff RS. Synthesis and exfoliation of isocyanate-
386 treated graphene oxide nanoplatelets. Carbon 2006; 44(15) 3342-3347.
387 [19] Kim DH, Yun YS, Jin HJ. Difference of dispersion behavior between graphene oxide
388 and oxidized carbon nanotubes in polar organic solvents. Current Applied Physics 2012;
389 12(3): 637-642.
390 [20] Kim H, Abdala AA, Macosko, CW. Graphene/polymer nanocomposites.
391 Macromolecules 2010; 43(16): 6515-6530.
392 [21] Du J, Cheng HM. The Fabrication, properties and uses of graphene/polymer composites
393 Macromol Chem Phy 2012; 213: 1060-1077.

394 [22] Thomas H R, Valles C, Young RJ, Kinloch IA, Wilson NR, Rourke PJ. Identifying the
395 fluorescence of graphene oxide. Journal of Mater Chem C 2013, 1: 338-342.
396 [23] Fan X, Peng W, Li Y, Wang S, Zhang G, Zhang F. Deoxygenation of exfoliated graphite
397 oxide under alkaline conditions: a green route to graphene preparation. Adv Mater 2008*;*
398 20: 4490-4493.
399 [24] Bai S, Shen X, Zhu G, Yuan A, Zhang J, Ji Z, Qiu D. The influence of wrinkling in
400 reduced graphene oxide on their adsorption and catalytic properties. Carbon 2013; 60:
401 157-168.
402 [25] Galpaya D, Wang M, Yan C, Liu M, Motta N, Waclawik ER. (2013) Fabrication and
403 mechanical and thermal behaviour of graphene oxide/epoxy nanocomposites. Journal of
404 Multifunctional Composites 2013, 1(2): 91-98.
405 [26]] Hsu TC. Adsorption of an acid dye onto fly ash. Fuel 2008; 87:3040-3045.
406 [27] Willner MR. Metal removable by sodium graphene oxide. Master of Science in
407 Environmental Engineering 2012, University of Notre Dame, Indiana.
408 [28] Li Z, Young RJ, Kinloch IA. Interfacial stress transfer in graphene oxide
409 nanocomposites. ACS Appl Mater Interfaces 2013; 5: 456-463..
410 [29] Zhao X, Zhang Q, Chen D. Enhanced mechanical properties of graphene-based
411 poly(vinyl alcohol) composites. Macromolecules 2010; 43: 2357–2363.
412 [30] Rafiee MA, Rafiee J, Srivastava I, Wang Z, Song H, Yu, ZZ, Koratkar N. Fracture and
413 fatigue in graphene nanocomposites. Small 2010; 6(2), 179–183.
414 [31] Rafiee MA, Rafiee J, Srivastava I, Wang Z, Song H, Yu ZZ, Koratkar N. Enhanced
415 mechanical properties of nanocomposites at low graphene content. ACS Nano 2009;
416 3(12): 3884-3890.

[32] Gong L, Kinloch IA, Young RJ, Riaz I, Jalil R, Novoselov KS. Interfacial stress transfer in a graphene monolayer nanocomposite. Advanced Materials 2010; 22(24): 2694–2697.

[33] Tapasztó L, Dumitrica T, Jin-Kim S, Nemes-Incze P, Hwang C, Biró LP. Break-down of continuum mechanics for nanometer-wavelength rippling of graphene. Nature Physics 2012; 8: 739-741.

[34] Graphene in composite materials: synthesis, characterization and applications. Edited by Koratkar N, March 2003, DEStech Publications, Inc.

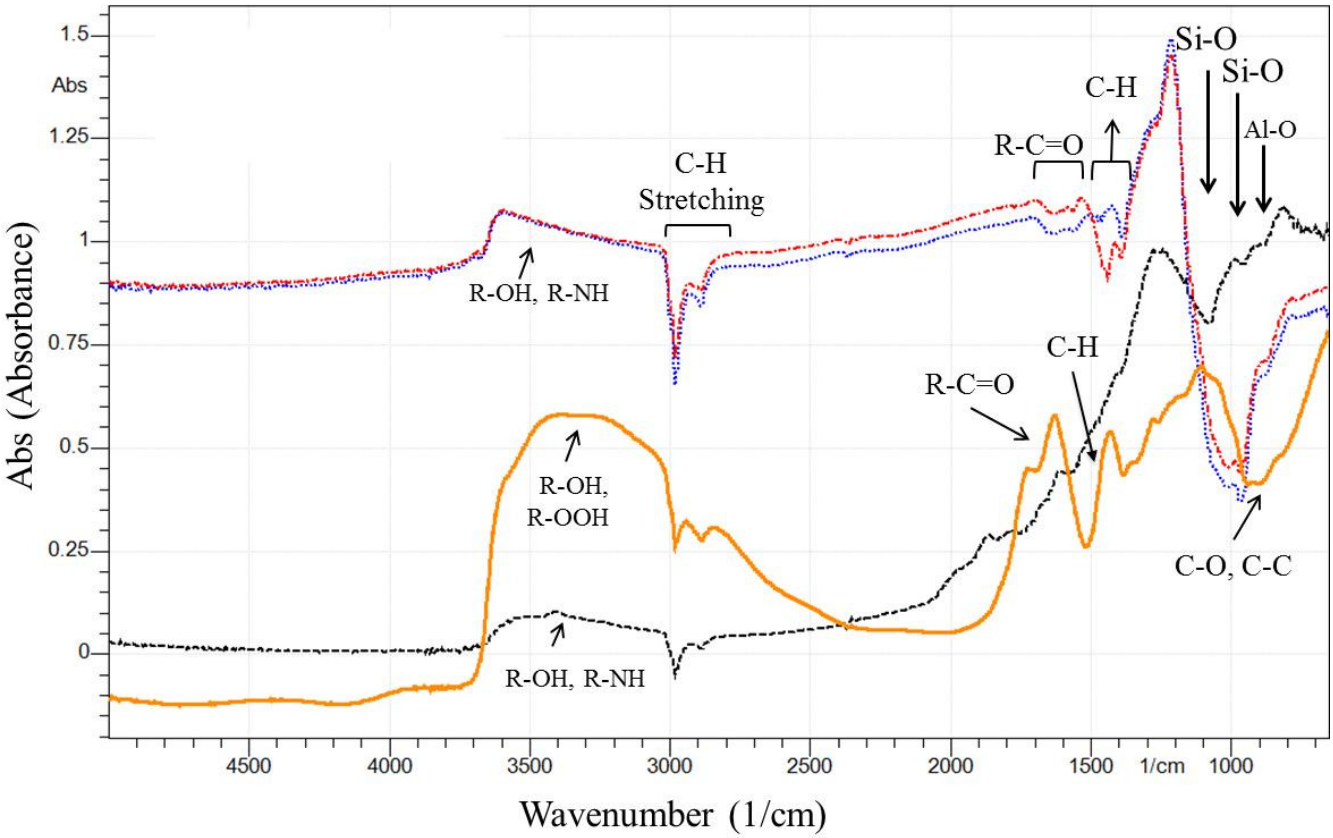

Fig. 1 – Diffuse FTIR spectra of fly ash (black line), un-reduced GO sheets (orange line), plain geopolymeric composites (red line) and rGO incorporated into the geopolymeric composites (blue line).

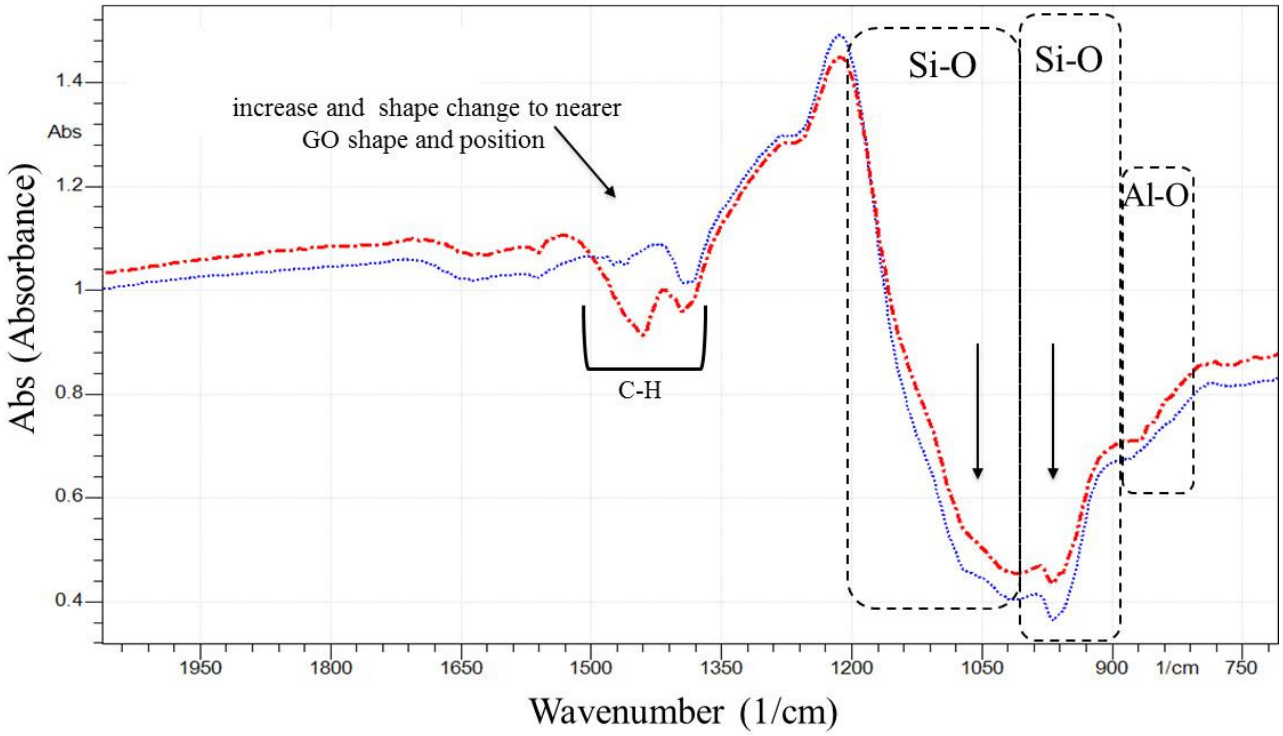

Fig.2- Diffuse FTIR spectra between 2000 and 650 1/cm of plain geopolymeric composites (red line) and rGO incorporated into the geopolymeric composites (blue line).

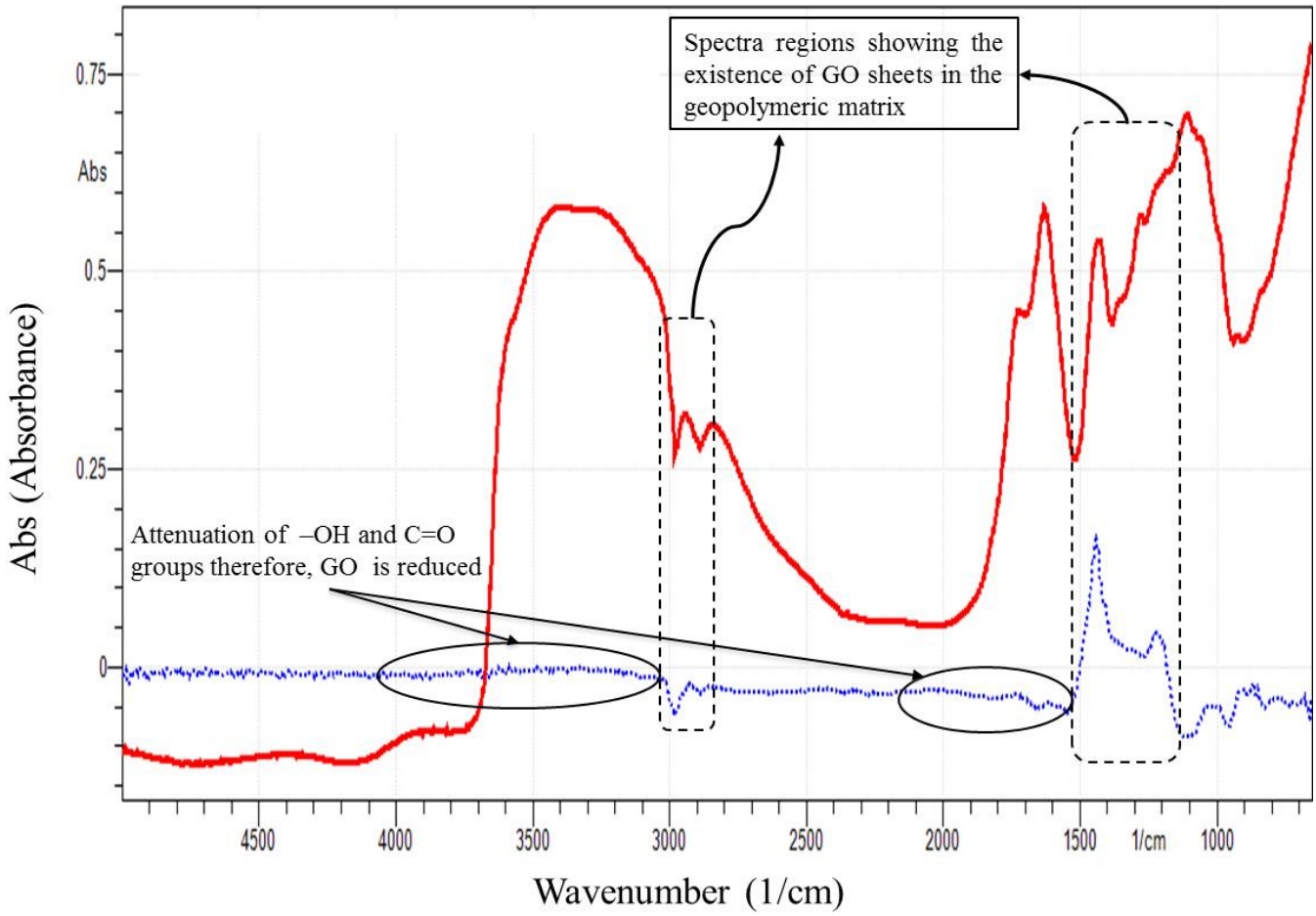

Fig. 3- Diffuse FTIR spectra of un-reduced GO (red line) in comparison to the difference spectra (blue line) of the geopolymer with and without rGO.

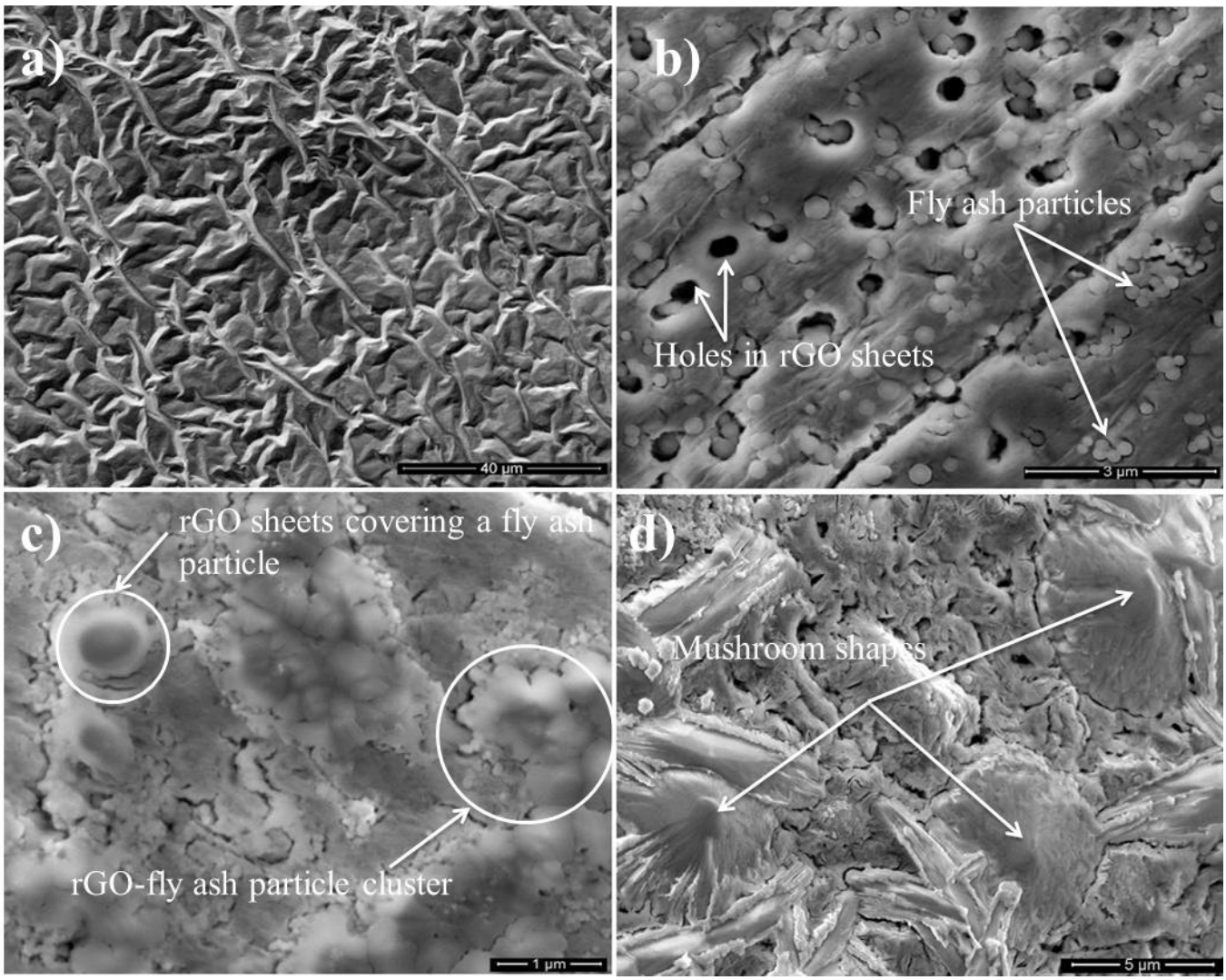

Fig.4 - SEM micrographs (a) morphology of rGO sheets (b) 0.35-wt% GO sheets interaction with submicron fly ash, (c) 0.35-wt% GO sheets covering submicron fly ash particles, (d) 0.35-wt% GO sheets interaction with larger fly ash particles.

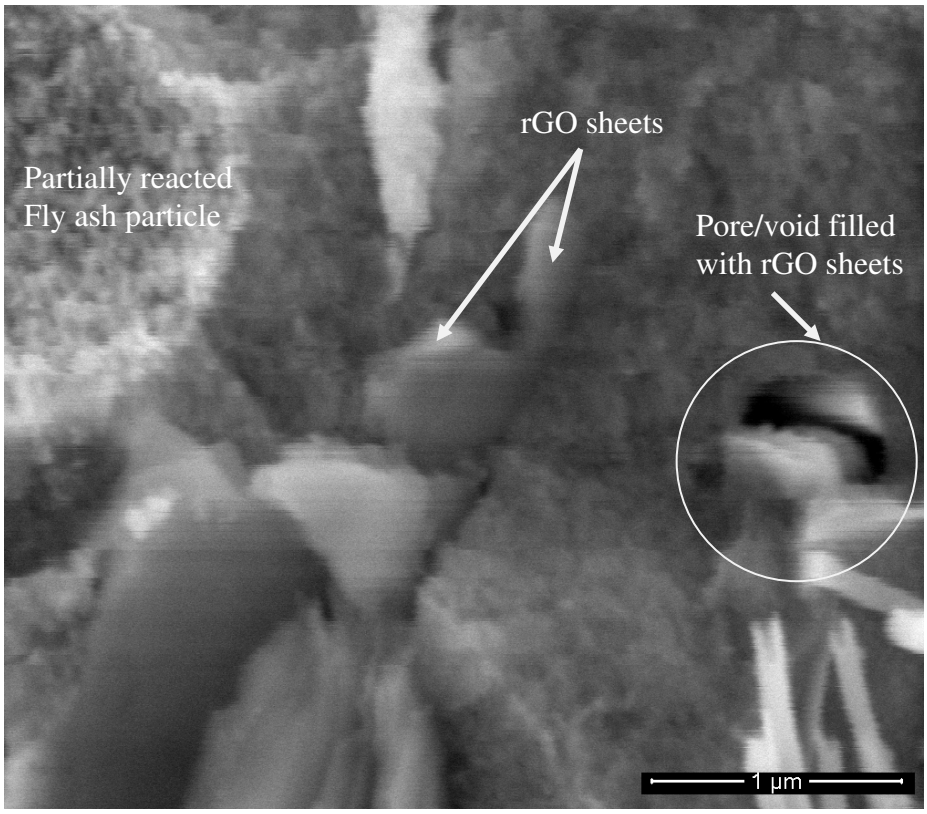

Fig. 5- SEM micrograph showing 0.5-wt% rGO sheets filling pores and voids.

.

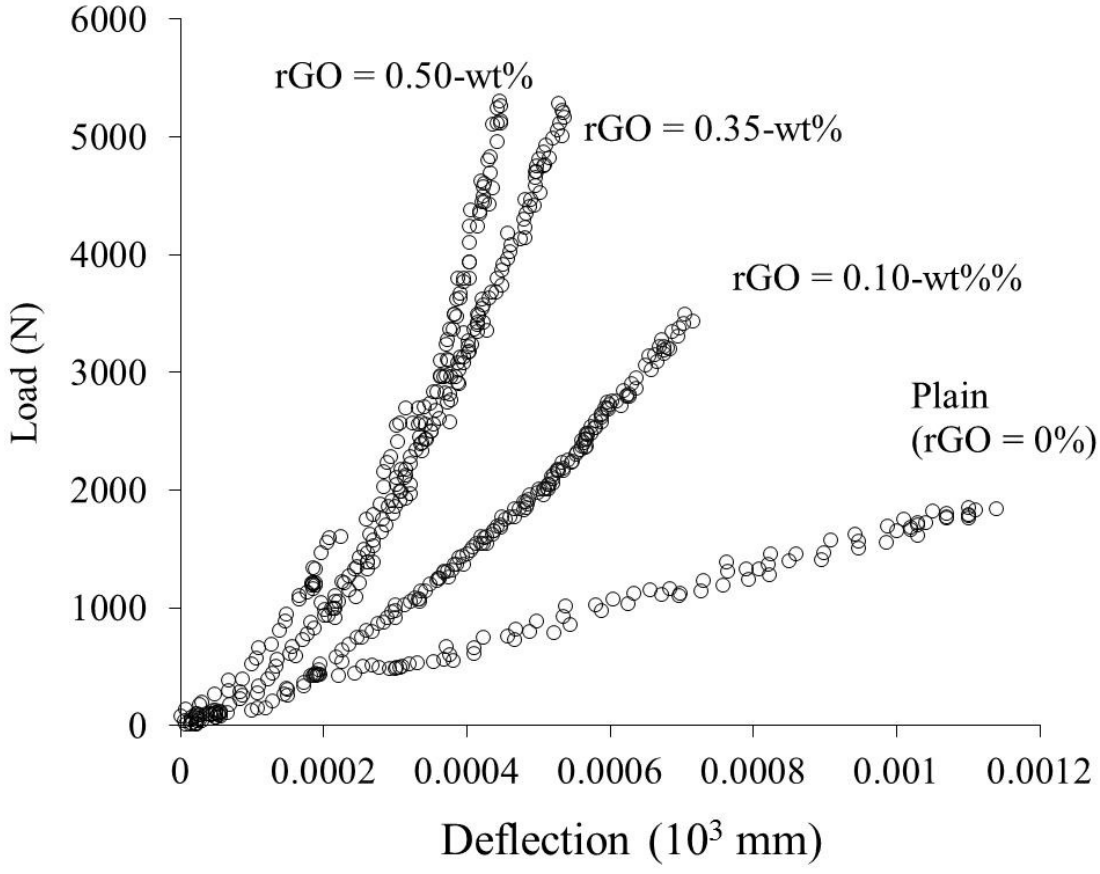

Fig.6-Load-deflection response of the rGO-geopolymeric composite beams.

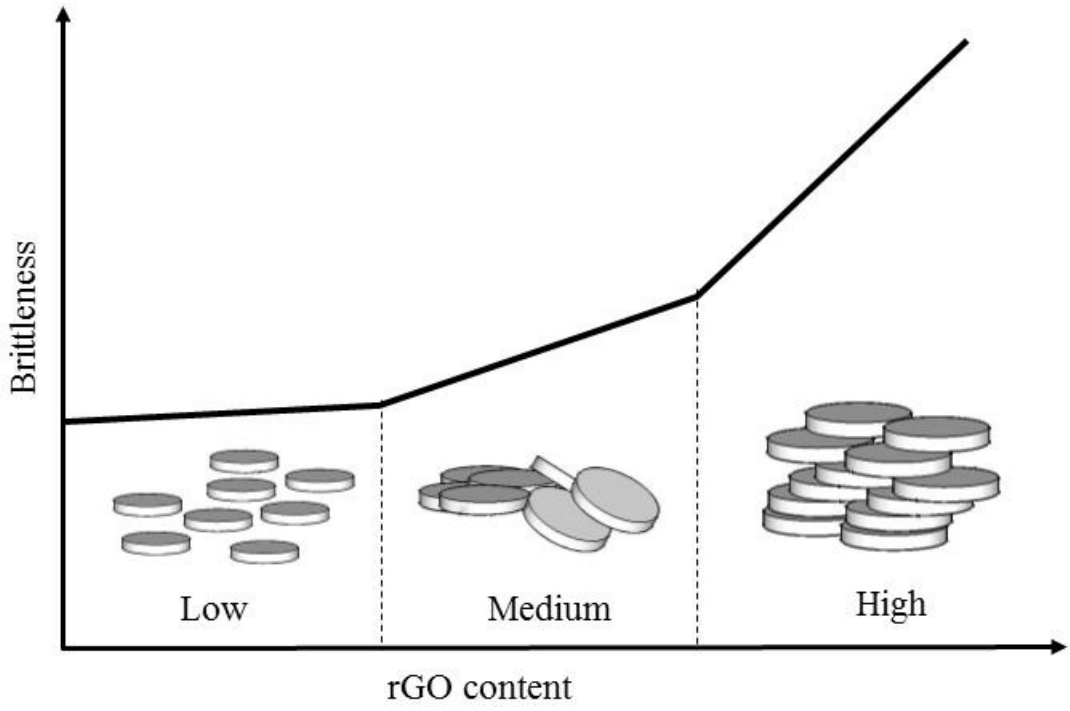

Fig. 7-Effect of rGO content on the brittleness of rGO-geopolymeric composites

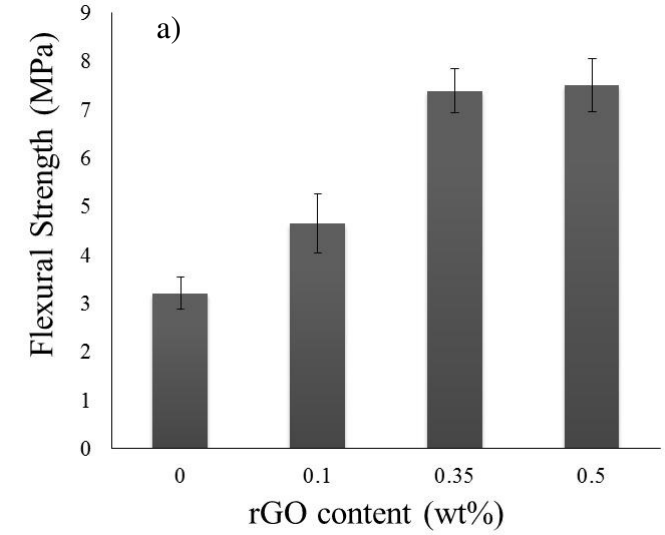

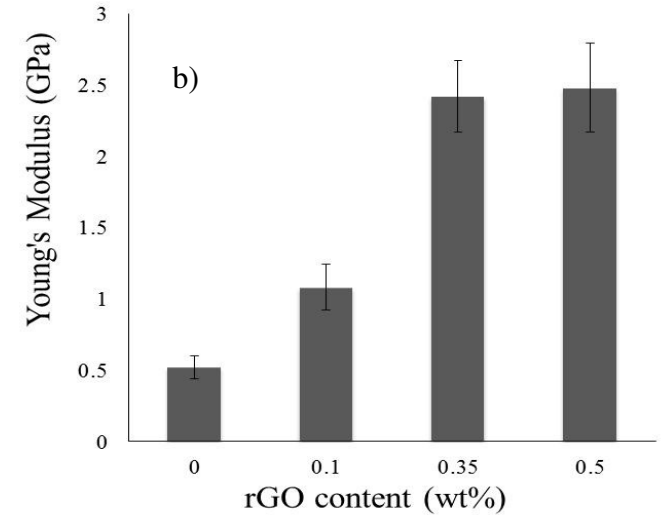

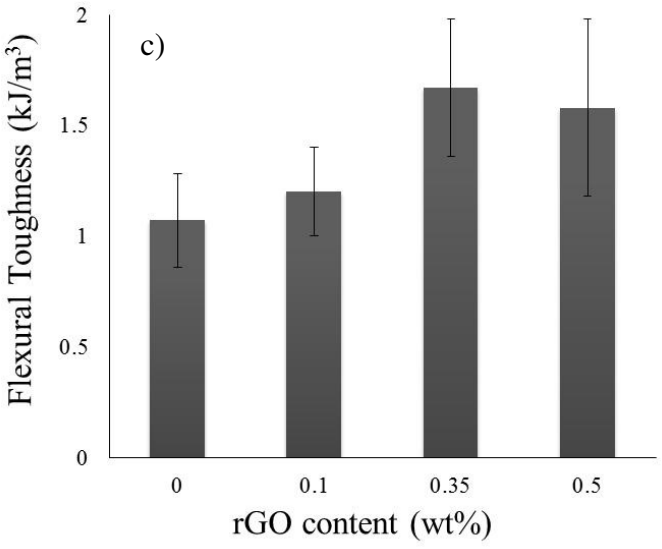

Fig.8- Mechanical properties of rGO-geopolymeric composites. a) flexural strength, b) Young's modulus, c) flexural toughness.

Table 1. Main chemical composition of fly ash (wt%)
(as provided by the supplier)

Element	Weight %
Silicon dioxide, SiO_2	53.50
Aluminium oxide, Al_2O_3	34.30
Iron oxide, Fe_2O_3	3.60
Calcium oxide, CaO	4.40
Loss of Ignition	2.00